

Article

Not peer-reviewed version

Back to the Metrics: Exploration of Distance Metrics in Anomaly Detection

[Yujing Lin](#) and [Xiaoqiang Li](#) *

Posted Date: 10 June 2024

doi: 10.20944/preprints202406.0529.v1

Keywords: image anomaly detection; defect detection; industrial manufacturing; distance metrics; anomaly score distribution





Preprints.org is a free multidiscipline platform providing preprint service that is dedicated to making early versions of research outputs permanently available and citable. Preprints posted at Preprints.org appear in Web of Science, Crossref, Google Scholar, Scilit, Europe PMC.

Copyright: This is an open access article distributed under the Creative Commons Attribution License which permits unrestricted use, distribution, and reproduction in any medium, provided the original work is properly cited.

Article

Back to the Metrics: Exploration of Distance Metrics in Anomaly Detection

Yujing Lin ¹ , and Xiaoqiang Li ^{1,*} 

School of Computer Engineering and Science, Shanghai University, Shanghai 200444, China;

* Correspondence: xqli@shu.edu.cn;

Abstract: With increasing research focus on industrial anomaly detection, numerous methods have emerged in this domain. Notably, memory bank-based approaches, coupled with kNN distance metrics, have demonstrated remarkable performance in anomaly detection (AD) and anomaly segmentation (AS). However, upon examination of the Back to the Feature (BTF) method applied to the MVTec-3D AD dataset, it was observed that while it exhibited exceptional segmentation performance, its detection performance was lacking. To address this discrepancy, this study base improves the implementation of BTF, especially the improvement of the anomaly score metric. It posits that different "clusters" necessitate distinct k values in kNN distance metrics. For simplify, this assumption is distilled into the proposition that AD and AS tasks impose differing requirements on the k value in kNN distance metrics. Consequently, the paper introduces the BTM method, which utilizes distinct distance metrics for AD and AS tasks. This innovative approach yields superior AD and AS performance (I-AUROC 93.0%, AURPO 96.9%, P-AUROC 99.5%), representing a substantial enhancement over the BTF method (I-AUROC 5.7% ↑, AURPO 0.5% ↑, P-AUROC 0.2% ↑).

Keywords: image anomaly detection; defect detection; industrial manufacturing; distance metrics; anomaly score distribution;

1. Introduction

Anomaly detection (AD) aims at finding instances that diverge from the "normal" data in the general sense[1–4]. Meanwhile, anomaly segmentation (AS) looks into specific anomalous instances and precisely delineating the abnormal regions, such as identifying the locations of abnormal pixels. The combined field of anomaly detection and segmentation (AD&S) plays a critical role in various applications, including industrial inspection, security surveillance, and medical image analysis [3,5,6].

2D Industrial Anomaly Detection With industrial anomaly detection becomes increasingly emphasized, datasets such as MVTec AD [5,6], BTAD [7], MTD [8], and MVTec LOCO AD [9] have been successively introduced. This has stimulated the development of industrial AD&S and facilitated the proposal of many novel anomaly AD&S methods. We categorize these methods into three main types:

1. **Supervised Learning:** These algorithms treat anomaly detection as an imbalanced binary classification problem. This approach suffers from the scarcity of abnormal samples and the high cost of labeling. To deal with the problems, various methods were proposed to generate anomalous samples so as to alleviate the labeling cost. For example, CutPaste[10] and DRAEM[11] manually construct anomalous samples; SimpleNet[12] samples anomalous features near positive sample features; NSA[13] and GRAD[14] synthesize anomalous samples based on normal samples. Despite the diversity of anomaly generation methods, they consistently fail to address the underlying issue of discrepancies between the distributions of generated and real data. [15–17]
2. **Unsupervised Learning:** These algorithms operate under the assumption that the data follow a normal distribution. For example, SROC [18] and SRR [19] rely on this assumption to identify and remove minor anomalies from the normal data. When combined with semi-supervised learning techniques, these algorithms achieve enhanced performance.
3. **Semi-supervised Learning:**

Concentration assumption, which suppose that the normal data are usually bounded if the features extracted are good enough, is commonly used when designing semi-supervised learning AD&S method. These algorithms requires only labels for normal data and assumes boundaries in the normal data distribution for anomaly detection. Examples include: Autoencoder-based [20–22], GAN-based [20,23–25], Flow-based [26–30], and SVDD-based [31–33]. Some memory bank based methods (MBBM) [16,17,34–37] that combine pre-trained features from deep neural networks with traditional semi-supervised algorithms have achieved particularly outstanding results and also possess strong interpretability. In rough chronological order, we summarize the main related algorithms as follows:

- (a) DN2 [34] was the first to use k-nearest neighbors (kNN) with deep pre-trained features for AD task, and introduces Group Anomaly Detection (GAD) [38]. After that, some works [16,17] fit Gaussian distributions to deep pre-trained features for anomaly scoring using Mahalanobis distance.
- (b) SPADE, building on DN2, [35] employs Feature Pyramid Matching to achieve image AD&S.
- (c) PaDiM [36] models pre-trained feature patches with Gaussian distributions for better AD&S performance.
- (d) Panda [33] sets subtasks based on pre-trained features for model tuning, to achieve better feature extraction and improve model performance.
- (e) PatchCore [37] and ReConPatch [39] have achieved excellent performance by utilizing downsampled pre-trained feature sets from the kNN method. They have consistently held top positions on the performance leaderboard for an extended period.

The aforementioned MBBM method is highly relevant to our study, yet aside from the initial discussion on distance metrics in the GAD problem by DN2, subsequent research has not specifically addressed this issue. Notably, PatchCore introduced a distance metric approach that has not been publicly released in the official GitHub repository, and the method is inadequately described in the literature. We will discuss this approach further in Section 2. More recently, the paper "Probabilistic transformation of outliers based on Distance" has done exploratory work based on previous MBBM. In conclusion, the author points out that the reweight strategy and downsampling method in the distance-based outlier detection method are worthy of further study [40]. This is very consistent with our findings on the MVTec-3D AD dataset.

3D Industrial Anomaly Detection To fill the gap in the 3D AD&S domain, the MVTec-3D AD [41] dataset along with its corresponding baseline algorithms and performance metrics were released to the public, which introducing new opportunities and challenges to industrial AD&S. In subsequent research, various novel methods have been developed and achieved notable results. These include methods based on teacher-student networks such as 3D-ST [42] and AST [43], methods leveraging the PatchCore scoring function like (Back to the Features) BTF [44] and M3DM [45], and methods focused on constructing anomalies such as 3DSR [46]. Additionally, approaches that utilize Neural Implicit Functions and pre-trained models, exemplified by Shape-Guided [47], have been introduced. These studies primarily aim to design new methods for 3D feature extraction and feature integration.

In the MVTec-3D AD dataset, it was observed that BTF achieved significant performance in terms of AS, but lagged in AD performance. Upon further investigation, it was found that methods such as ReConPatch, BTF, and M3DM perform anomaly scoring calculations based on the PatchCore method. These algorithms differ significantly from the initially proposed image domain anomaly scoring algorithm based on kNN [34] and the traditional kNN classification algorithm [48]. The authors lacked specific discussion when introducing these differences. In this paper, the distance measures involved in these algorithms are compared and analyzed, and their advantages and disadvantages are pointed out. According to these advantages and disadvantages, combined with our improvement of the existing MBBM method, we propose a method that uses different anomaly scores in the AD and AS phases, respectively.

The key contributions of this work include:

1. **Methodological Clarification (PatchCore and BTF):** We compare and analyze the theoretical framework and official implementation of PatchCore and BTF, then identify and correct some careless errors found in the paper or code, while clarifying the framework of BTM. The correction of the details is important for subsequent research.
2. **Distance Metric Analysis:** We visualized and analyzed the distance measure in the anomaly scoring algorithm, providing initial insights into its strengths and weaknesses. Based on these analyses, we also propose some assumption.
3. **Method Proposed:** On the basis of BTF, a method named Back to the Metrics (BTM) is proposed in Section 2.1, which achieves the performance improvement of (I-AUROC 5.7% ↑, AURPO 0.5% ↑, and P-AUROC 0.2% ↑). It is also competitive against other leading methods.

This paper is divided into three parts:

1. Section 2 optimizes the nearest neighbor feature fusion, feature alignment and distance metric based on BTF, and proposes the BTM method. Then, the basis of modification is introduced, including a summary of the framework of MBBM method, and an analysis of the implementation details of MBBM (anomaly score calculation, feature fusion and downsampling method)
2. Section 3 first provides comprehensive information on the datasets used, code implementation details, and parameters used. On this basis, it then compares the performance of the proposed method in section 2 using real data sets
3. Section 4 summarizes the conclusions drawn in this work and explores future research directions.

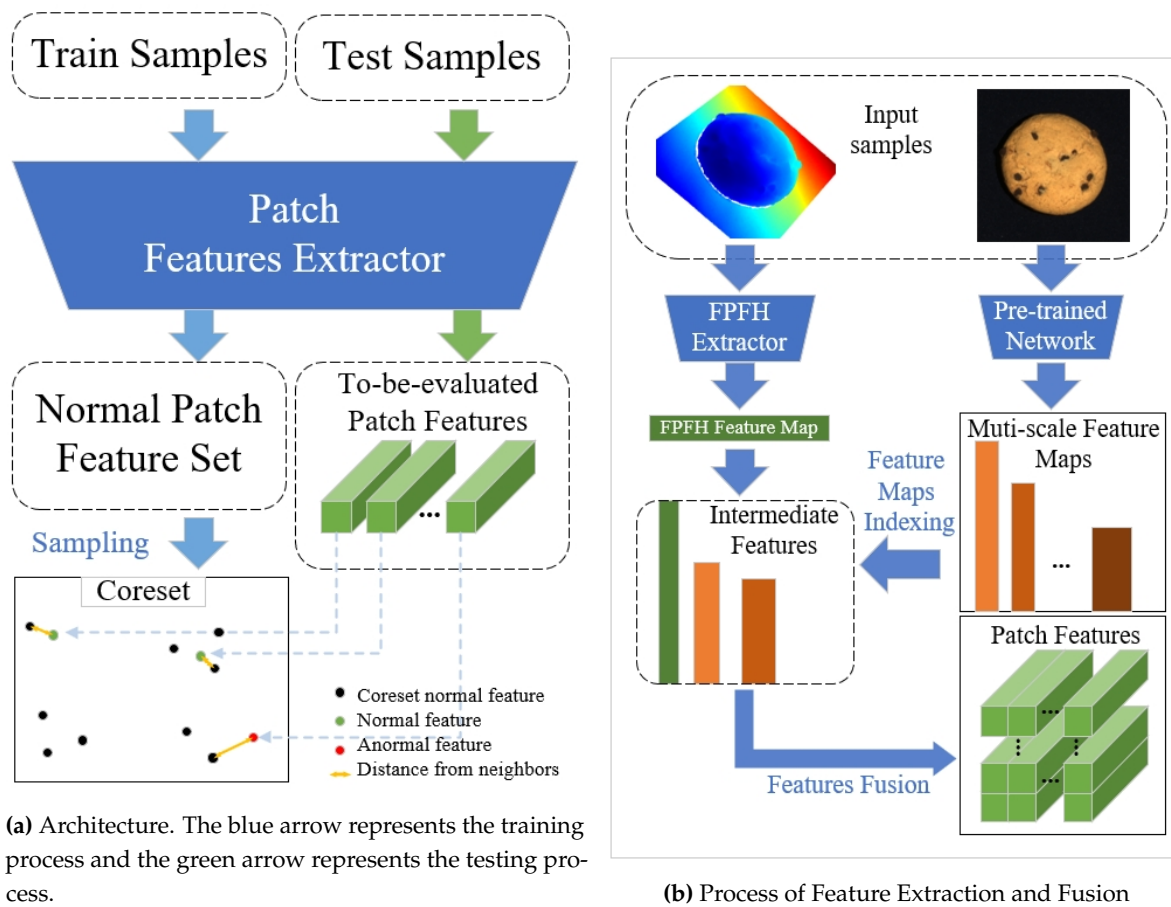
2. Methodology

2.1. Back to the Metric

2.1.1. Framework

This chapter describes the general framework of BTM method through the summary of MBBM method.

In BTM, we have followed the traditional framework of MBBM framework illustrated in Figure 1. Specifically, Figure 1a is dedicated to introducing MBBM. For methods focused solely on anomaly detection (AD), it can be elucidated that the Patch Features Extractor (PFE) extracts only one feature for each sample. In other words, such methods treat the entire image as a single patch. Figure 1b shows the feature extraction process of BTM method on MVTec-3D AD dataset. The process depicted is consistent with BTF, with variations noted in Section 3.3 and Section 2.1.2.



(a) Architecture. The blue arrow represents the training process and the green arrow represents the testing process.

(b) Process of Feature Extraction and Fusion

Figure 1. (a) The Architecture of the Back to the Metrics(BTM). (b) Process of Feature Extraction and Fusion with Fast Point Feature Histograms (FPFH) and Pre-trained Network

2.1.2. Optimization

On the framework shown in Figure 1, we opt to use kNN Squared Distance Mean Metrics as the anomaly score calculation function for AS tasks, and employ nearest neighbor Metrics to compute image-level anomaly scores. We term this approach BTM and conduct AD&S experiments on the MVTec-3D AD dataset.

Building upon BTF, we referenced DN2's work on GAD and, considering the alignment requirements between images and features, utilized a mean convolution kernel with kernel-size=3, stride=1, and padding=1 to fuse neighboring features. For the sake of logical correctness and code parallelism, we replaced the elliptical Gaussian blur kernel used in computing AS anomaly scores with a Gaussian blur kernel of kernel-size=15 and sigma=(4,4), directly applicable to tensors. We'll get into the details of why these changes were made in a later section.

2.2. The Structure of Memory Bank Based Methods(MBBM)

2.2.1. Anomaly Score Metrics

Traditional kNN algorithm is a classification algorithm based on similarity metrics. It determines the category of a new sample by selecting kNN to vote, where k is usually chosen as an odd number to avoid ties during the voting process[48]. In semi-supervised anomaly detection, anomalous samples do not appear in the training set. In contrast, the MBBM considers the influence of multiple different normal samples in the anomaly scoring function through techniques like re-weighting.

DN2 is the first model to introduce a kNN-based method in industrial image anomaly detection, scoring image anomalies using Equation 1.

$$s = d(x) = \frac{1}{k} \sum_{f \in \mathcal{N}_k(f_x)} \|f - f_x\|_2 \quad (1)$$

The symbol $\mathcal{N}_k(f_x)$ represents the set of k nearest feature vectors to f_x within the training set F_{train} . The anomaly score s of the test image is denoted by the distance function $d(x)$, which is the average sum of squared Euclidean distances between the feature vector f_x and the feature vectors f in its kNN $\mathcal{N}_k(f_x)$. The rule with $k = 1$ is commonly referred to as the nearest-neighbor rule.[48]

Work such as SPADE further extends DN2 to AS tasks. For a image sample that is divided into I rows and J columns: $f_{i,j}$ represents the feature extracted from the patch at the i th row and j th column, and

$$F = \{f_{i,j} \mid 0 \leq i < I, 0 \leq j < J\}$$

represents the set of features for the entire image; let $s_{i,j}$ represent the anomaly score of the patch at the i th row and j th column; let \mathcal{M} represent the coreset of features obtained by applying a greedy algorithm for subsampling on the set of patch features from all images in the training set; let $\mathcal{N}_k(f_y)$ represent the set of k nearest features to f_y in \mathcal{M} .

$$s_{i,j} = \frac{1}{k} \sum_{f \in \mathcal{N}_k(f_{i,j})} \|f - f_{i,j}\|_2 \quad (2)$$

For each image, PatchCore's official code uses Equation 2 for AS anomaly score calculation, where $k = 1$ in the paper, which can be represented by Equation 3.

$$s_{i,j} = \min_{m \in \mathcal{M}} \|m - f_{i,j}\|_2 \quad (3)$$

PatchCore defines the maximum distance score s^* of a test image, which can be expressed as Equation 4 or more closely to the original text as Appendix 6 (less rigorous). Here, f_{i^*,j^*} is the feature in the test image with the highest anomaly score, and m^* is the feature in the core set \mathcal{M} that is nearest to f_{i^*,j^*} .

$$s^* = \max_{0 \leq i < I, 0 \leq j < J} s_{i,j} \quad (4)$$

It is noteworthy that, in conjunction with the understanding of Equation 3 and Equation 4, we propose that the terms m^* and f_{i^*,j^*} in Equation 11 and Equation 12 need to be redefined as shown in Equation 5. Here, $m_{i,j}$ represents the nearest neighbor of f_{i^*,j^*} within \mathcal{M} , and S_{fm} denotes the set composed of tuples, each consisting of all patch features from an image and their respective nearest neighbors in \mathcal{M} .

$$\begin{aligned} m_{i,j} &= \arg \min_{m \in \mathcal{M}} \|m - f_{i,j}\|_2 \\ S_{fm} &= \{(f_{i,j}, m_{i,j}) \mid 0 \leq i < I, 0 \leq j < J\} \\ (f_{i^*,j^*}, m^*) &= \arg \max_{(f_{i,j}, m_{i,j}) \in S_{fm}} \|m_{i,j} - f_{i,j}\|_2 \end{aligned} \quad (5)$$

$$w = \left(1 - \frac{\exp(\|f_{i^*,j^*} - m^*\|_2)}{\sum_{m \in \mathcal{N}_k(m^*)} \exp(\|f_{i^*,j^*} - m\|_2)} \right) \quad (6)$$

$$s = w \times s^* \quad (7)$$

To make the image anomaly scoring results more robust [37], PatchCore employs the weights w from Equation 6 to reweight s^* as the anomaly score, as shown in Equation 7. BTF and M3DM both implemented Equation 6 in their code, but M3DM employed complex methods such as reweighting and One-Class Support Vector Machines for anomaly score re-calculation.

$$\begin{aligned}
 \alpha_1 &= \frac{\exp(\|f_{i^*,j^*} - m^*\|_2)}{\sum_{m \in \mathcal{N}_k(m^*)} \exp(\|f_{i^*,j^*} - m\|_2)} \\
 \alpha_2 &= \sum_{m \in \mathcal{N}_k(m^*)} \exp(\|f_{i^*,j^*} - m\|_2) \\
 &= \sum_{m \in \mathcal{N}_k(m^*)} \exp(\sqrt{f_{i^*,j^*}^T f_{i^*,j^*} - 2f_{i^*,j^*}^T m + m^T m}) \\
 &= \sum_{m \in \mathcal{N}_k(m^*)} \exp(\sqrt{\|f_{i^*,j^*}\|_2^2 - 2f_{i^*,j^*}^T m + \|m\|_2^2}) \\
 \beta_1 &= \|f_{i^*,j^*}\|_2^2 \\
 \beta_2 &= \|m\|_2^2 \\
 \beta_3 &= f_{i^*,j^*}^T m
 \end{aligned} \tag{8}$$

To facilitate further analysis, we define partial component factors (or terms) α_1 and α_2 of the variable w as shown in Equation 8. Additionally, factors β_1 , β_2 , and β_3 expanded from α_2 are also defined in Equation 8. The exponential function $\exp(\cdot)$ and the square root function $\sqrt{\cdot}$ are monotonically increasing and therefore not specifically considered.

In summary, the officially released PatchCore-derived methods currently primarily utilize the anomaly scores Equation 2 and Equation 3 for the AS task, and Equation 2, Equation 3, and Equation 5 for the AD task.

2.2.2. Feature Fusion

In pure image anomaly detection (AD) tasks, the issue of feature fusion is not inherently involved. However, DN2 explored it as a GAD problem: as shown in Figure 2, DN2 compared three methods of feature fusion—concatenate, max, and mean—and found that using mean for feature fusion combined with the kNN anomaly score calculation algorithm resulted in the best ROCAUC performance. In contrast, the performance of the concatenate method in terms of ROCAUC first increased and then decreased with the enlargement of the group size, which provides some inspiration for feature fusion in subsequent work. This experiment offers some inspiration for feature fusion methods in subsequent work.

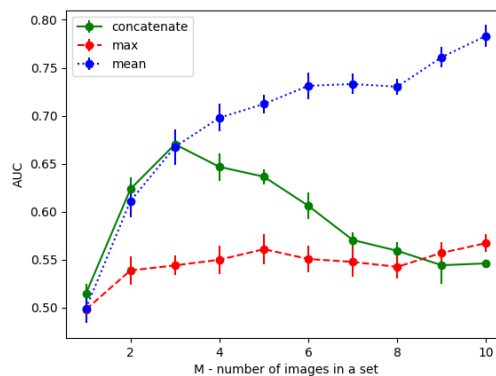


Figure 2. Performance comparison of anomaly detection methods using feature concatenation, max pooling, and mean pooling with varying numbers of images per group[34].

In the anomaly score (AS) of methods derived from PatchCore, two variants of feature fusion appear: 1) On the MVTec-3D AD dataset, the PatchCore code upsamples the high-level feature map to the same resolution as the low-level features using bilinear interpolation, then maps different levels to the same dimension (e.g., hyperparameter 1024), concatenates them together, and finally maps them to a feature vector of a specific dimension. 2) On 3D datasets, BTF and M3DM first use the mean method to perform domain feature fusion for different layer features (including RBB multi-scale features and geometric features), then the high-level feature map is upsampled to the same resolution as the low-level features using bilinear interpolation, and finally, the features from all layers are concatenated together to generate a feature vector.

Overall, the fusion of features from the same modality, such as the fusion of features from the same spatial domain, can be approached as a GAD problem, where using the mean method can yield better performance, especially when many features are involved. On the other hand, for the fusion of features from different modalities, including different scales and different characteristics, concatenation is a more common choice. More sophisticated and complex feature fusion techniques, such as those used by M3DM, are beyond the scope of this discussion.

Referring to DN2's work on GAD, in BTM we make the mean convolution kernel of size 3 and step 1 perform neighbor feature fusion, which is the same as in BTF. The difference is, given the feature alignment, we add a padding of size 1 to the convolution kernel. For features other than nearest neighbor features, we simply use concatenate as a feature fusion method.

2.2.3. the Iterative Greedy Approximation Algorithm

Both PatchCore and BTF utilize the Iterative Greedy Approximation (IGA) algorithm [49] to subsample the memory bank. IGA significantly addresses the issue of overemphasis on outlier samples in both active learning and anomaly detection scenarios. This method ensures the coverage, representativeness, and information complexity of the coreset samples. However, it is worth noting that in active learning, the normalcy of outliers is not a primary concern, whereas in anomaly detection, it is important.

The IGA algorithm tends to collect samples at the edges of sample clusters, typically high-frequency samples around low-frequency regions. Based on this characteristics of the IGA algorithm, we have the following assumption:

Assumption 1. *If there are abnormal samples in the training set, they are likely to be captured by IGA and become outliers (considered normal) in the core set.*

Assumption 2. *The low-frequency areas near high-frequency features (The boundary of the sample cluster), data points are likely to be outliers and should receive higher anomaly scores.*

2.3. Visualization Analysis of Different Metrics

In MBBM, the interaction between the anomaly score calculation function and feature engineering ultimately affects the calculation of anomaly scores. In existing research on image anomaly detection, the evaluation of anomaly score calculation functions is typically manifested as performance metrics on specific datasets. However, this is far from sufficient [40]. Considering the inherent flaws of real datasets and the significant impact of complex variable interactions on results, we simulate sample distributions in two-dimensional space to facilitate the visual analysis of anomaly score functions.

$$\begin{aligned} v_x &= \{x \in \mathbb{R} \mid x = x_0 + 0.005n, n \in \mathbb{N}, 0 \leq n < x_1\} \\ v_y &= \{y \in \mathbb{R} \mid y = y_0 + 0.005n, n \in \mathbb{N}, 0 \leq n < y_1\} \\ \text{Grid} &= v \times v, \quad \text{Grid} \in \mathbb{R}^{\lfloor (x_1 - x_0)(y_1 - y_0) \rfloor / 0.005 \times 2} \end{aligned} \quad (9)$$

As shown in Equation 9, this study uses v_x and v_y to respectively denote one-dimensional grid vectors along the x and y axes within the visualization region ($x_0 < x < x_1, y_0 < y < y_1$), and employs *Grid* to represent the two-dimensional spatial vector for visualization. We employ random sampling within the *Grid* to generate a core set $\in \mathbb{R}^{n \times 2}$, and subsequently visualize the gradient of anomaly scores within the *Grid* range.

The set $dists = \{(\|x - c\|_2) \mid x \in Grid, c \in coreset\}$ denotes the Euclidean distance between the points (x, y) in *Grid* and points c in *coreset*. By substituting *dists* into the corresponding formula, one can obtain the anomaly score or anomaly score weights Z , which are ultimately used to draw contours. Both *dists* and the anomaly scores can be obtained through parallel computation.

2.3.1. k-Nearest Neighbor Squared Distance Mean

When $k = 1$, as shown in Figure 3a, the algorithm ensures adequate sample coverage and representativeness. As k increases, as illustrated in Figure 3, the coverage and representativeness of outlier points significantly decrease, while the robustness of the anomaly score calculation function to outlier points slightly improves.

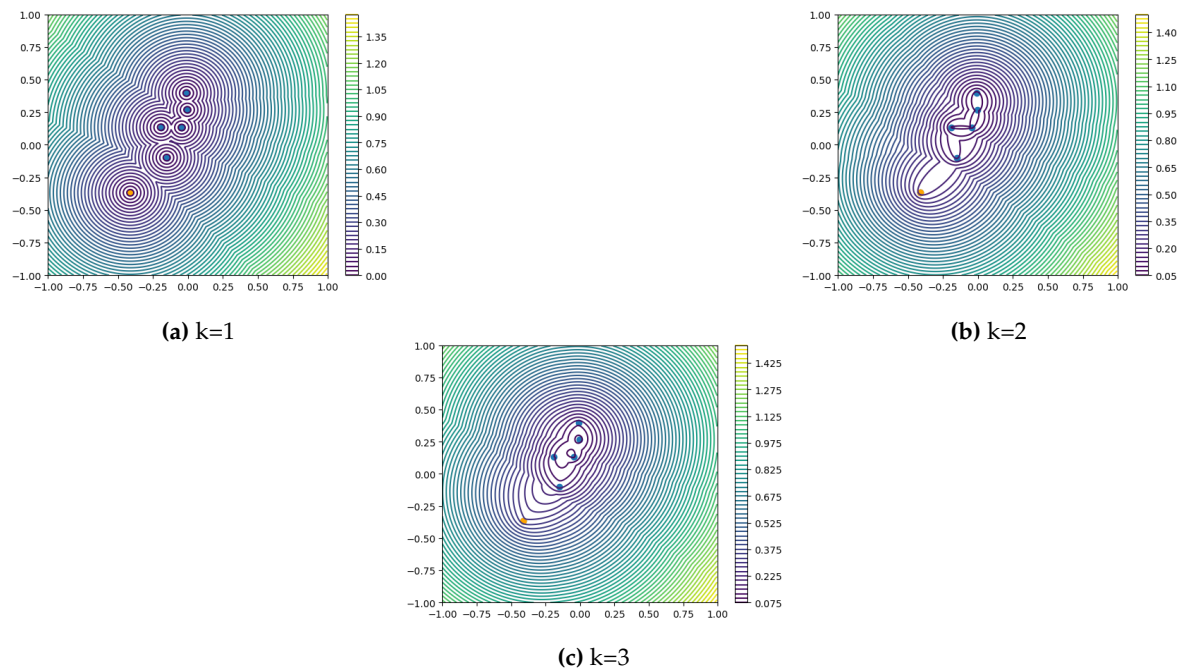


Figure 3. Gradient plots of Equation 2 for anomaly scores under simulated coreset with different values of k . Orange dots represent outliers.

Larger k values can increase the robustness of the model and reduce the influence of outliers, but at the expense of sample representativeness and coverage. When $k > 1$, we see a score distribution that conforms to Assumption 2. When the number of test samples is large enough and most of them are normal, it is a good choice to increase the k value appropriately to increase the robustness of the abnormal samples that may be introduced by Assumption 1. This fits the scenario of the AS task.

However, as we can see from the graph 3b. When k increases, there will be many "gullies" in the gradient plot of the abnormal fraction function. These "gullies" exist regardless of whether the outliers are normal or abnormal. Gullies "have no distinguishing power for anomalies. When Patch Core and BTF process AD tasks, the patch with the highest anomaly score plays a decisive role. In cases where a known sample is likely to be an anomaly (has a high probability of not being affected by outliers and reducing the anomaly score), the presence of these gullies is not conducive to anomaly summoning.

To sum up, MBBM uses k-nearest Neighbor Squared Distance Mean to measure the k value that may be needed for processing AS tasks. It is best to keep $k=1$ when processing AD tasks.

2.3.2. PatchCore Anomaly Score Calculation Function

The function composition of α_1 resembles Softmax. As shown in Figure 4, α_1 has larger values at the boundaries of the sample coverage area. As k increases, the maximum value of α_1 first decreases rapidly and then decreases slowly, approximately inversely proportional to k . Combining Equation 7 and Equation 8, we can observe that as k increases, the weight w tends to approach 1, and the influence of distance variance on the final anomaly score decreases.

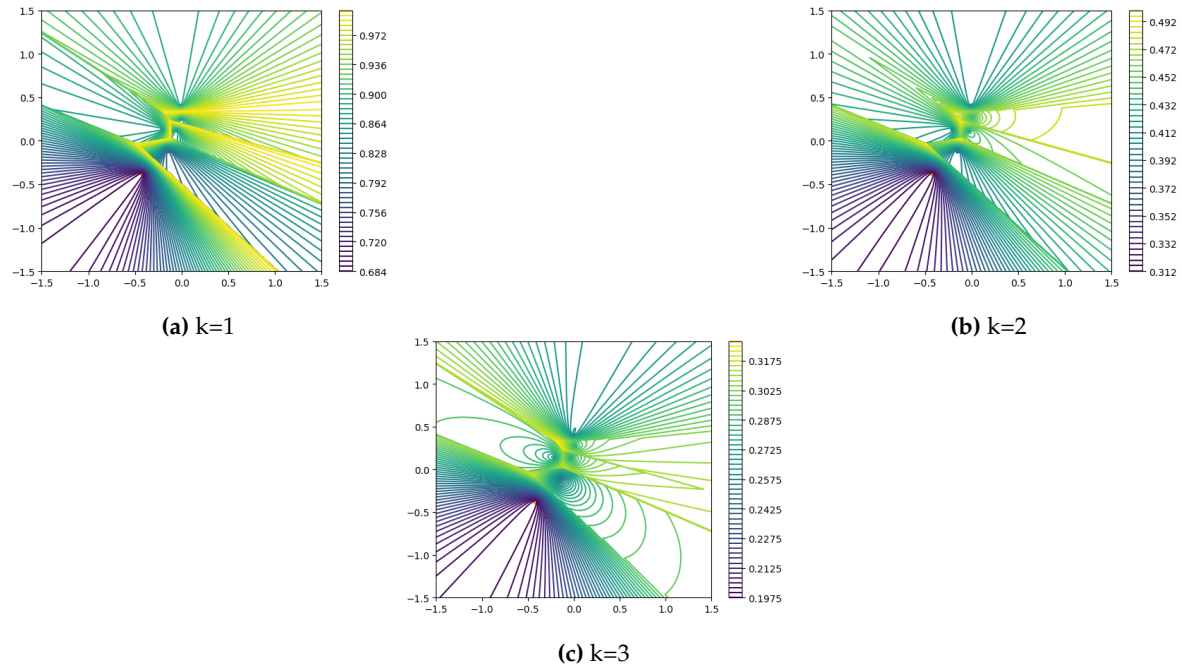


Figure 4. Gradient plots of the α_1 of Equation 8 under simulated coreset with different values of k . Orange dots represent outliers.

Figures 5 and 6 illustrate the behavior of s and w in Equation 7. w increases with the increase of k , while its factor α_1 decreases significantly. Except for Figure 5a, which exhibits a bizarre distribution of anomalies due to excessive influence from α_1 , assuming a randomly distributed sample set, both Figure 5a and Figure 5a are relatively reasonable: they conform to Assumption 2. If the outliers in the normal samples are marginal samples of this cluster, the gradient of anomaly scores on the outlier side is larger.

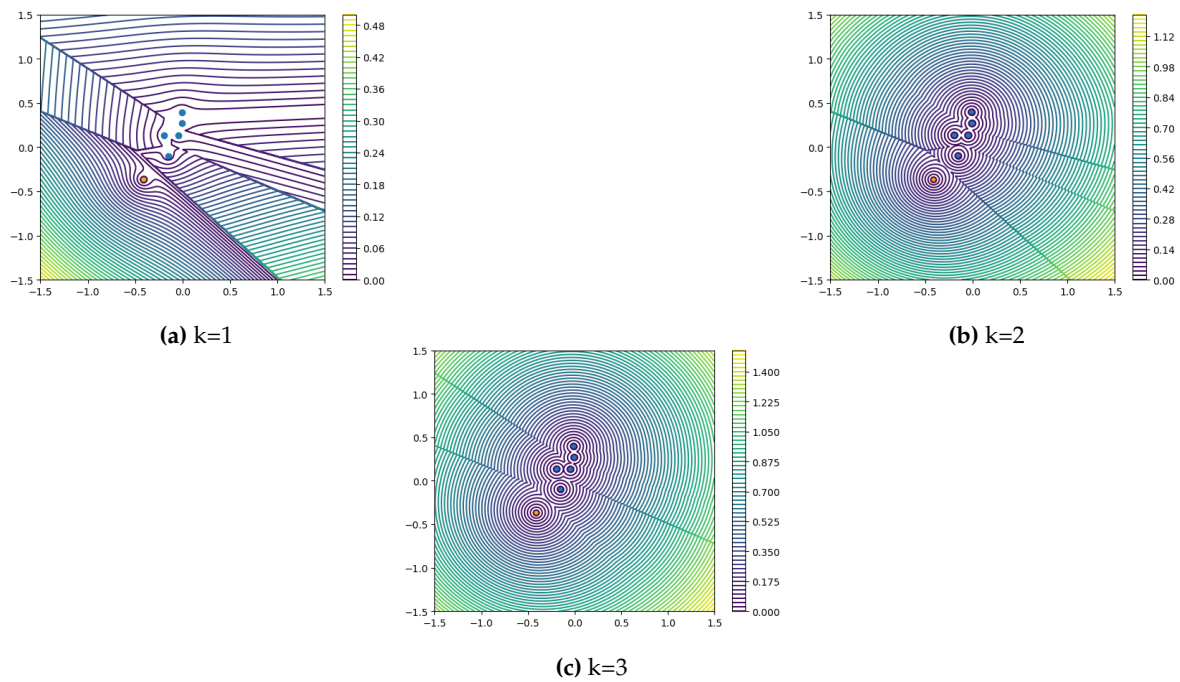


Figure 5. Gradient plots of Equation 7 for anomaly scores under simulated coresets with different values of k . Orange dots represent outliers.

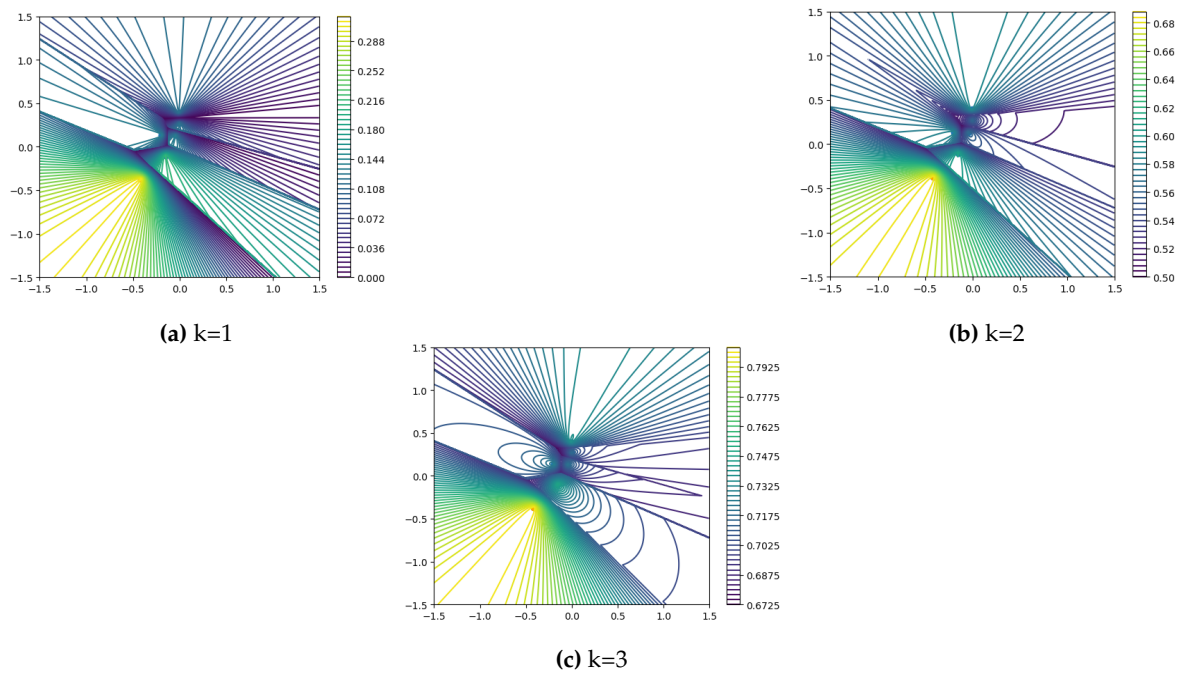


Figure 6. Gradient plots of the weight values of Equation 7 under simulated coresets with different values of k . Orange dots represent outliers.

In other words, w induces a subtle merging phenomenon in the distribution of anomaly scores for the k nearest neighbors of each point. This has adverse effects on the distribution of anomaly scores for clusters with a size less than or equal to k .

As shown in Figure 7b, when $k = 2$, the distribution of anomaly scores around the cluster composed of 3 sample points on the right side of the image does not exhibit significant inward shifting, forming a closed whole. Around the cluster composed of 2 sample points in the middle, a slight phenomenon of shifting towards the right side appears. While around the cluster composed of 1

sample point on the left side, there is a clear tendency for merging towards the right side. All clusters shown in Figure 7b exhibit slight merging phenomena. These merging or shifting phenomena are inconsistent with our assumptions.

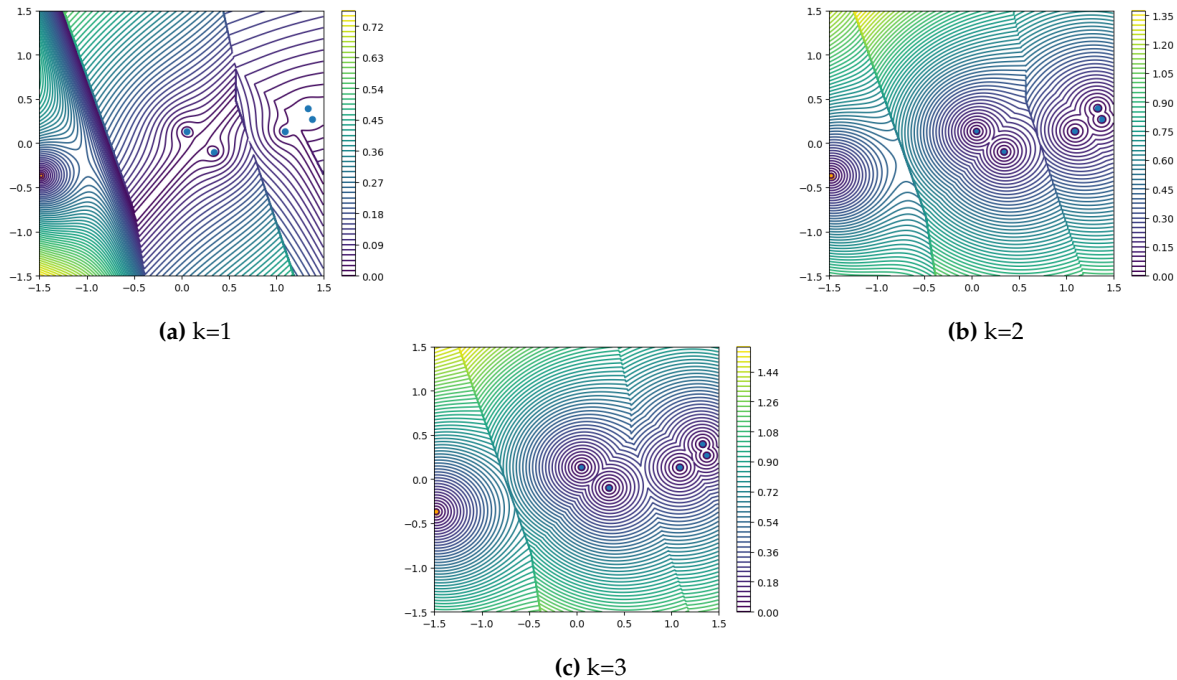


Figure 7. Enlarge the abscissa of the six samples in the coreset in Figure 5 by a factor of 7, dividing them into three clusters consisting of 1, 2, and 3 points, respectively, assuming they are samples sampled from the edges of three distribution clusters.

2.3.3. Summarize

In summary, the k-Nearest Neighbor Squared Distance Mean Score Calculation Function has obvious drawbacks when $k > 1$, but it exhibits better universality when $k = 1$. The PatchCore Anomaly Score Calculation Function can have better distribution patterns of anomaly scores in certain situations, but it imposes stringent requirements on the sampling method and the distribution of sampling results. When using the kNN distance metric to calculate the anomaly score, k needs to be smaller than the number of samples in the cluster, and the anomaly detection performance is best when k is close to the number of samples in the cluster. Accounting for the above visual analysis results, as shown in Equation 10, we define memory bank \mathcal{M}' as a set consisting of many clusters \mathcal{C} , each of which consists of kNN samples. In the equation, d should be defined based on empirical observations. Choosing a suitable k for each cluster in the anomaly scoring phase is noteworthy. However, for computational and implementation convenience, we simply assume that the k values of \mathcal{C} in \mathcal{M}' close to the abnormal samples of the test set are small, while the k values of other \mathcal{C} are large.

$$\begin{aligned}
 \mathcal{M}' = \{ & \\
 & \mathcal{C}_1, \mathcal{C}_2, \dots, \mathcal{C}_n \mid n \in \mathbb{Z}^+, \\
 & (\forall c \in \mathcal{C}_n, \exists c' \in \mathcal{C}_n \setminus \{c\}, \text{dist}(c, c') \leq d), \\
 & (\forall c \in \mathcal{C}_n, \forall c' \in \mathcal{M} \setminus \mathcal{C}_n, \text{dist}(c, c') > d) \\
 & \} \\
 \mathcal{M} = \bigcup_{\mathcal{C} \in \mathcal{M}'} & \mathcal{C}
 \end{aligned} \tag{10}$$

We pay more attention to abnormal samples in the anomaly detection (AD) task, while normal samples are predominant in the anomaly scoring (AS) task. Therefore, we should set different values of k for anomaly score calculation in AD and AS. Specifically, a smaller k value is designed for AD anomaly score calculation, and a larger k value is designed for AS anomaly score calculation.

3. Experiments

3.1. Datasets

The MVTec AD dataset is a comprehensive benchmark dataset for evaluating anomaly detection algorithms in industrial inspection scenarios. It consists of over 5,000 high-resolution color images across 15 different object and texture categories. The dataset includes both normal images for training and validation, as well as anomalous images for testing, with various types of real-world defects such as scratches, dents, and contaminations. The objects and textures in the dataset exhibit a range of complexities and challenges for anomaly detection, making it a valuable resource for developing and assessing the performance of unsupervised and semi-supervised anomaly detection methods in the context of manufacturing and quality control[5,6].

The MVTec-3D AD dataset comprises 4,147 high-resolution industrial 3D scans across 10 object categories. It includes anomaly-free scans for training and validation, as well as test samples with various real-world anomalies like scratches, dents, and contaminations. The objects range from those with natural variations (bagel, carrot, cookie, peach, potato) to standardized but deformable ones (foam, rope, tire) and rigid ones (cable gland, dowel). The dataset is designed for unsupervised anomaly detection in industrial inspection scenarios, featuring 41 types of anomalies[41].

3.2. Evaluation Metrics

This work compares the I-AUROC[5,6] and P-AUROC[5,6] performance with PatchCore on the MVTec AD dataset, and with BTF and M3dM on the MVTec-3D AD dataset, with the P-AUROC (integration upper limit set to 0.3)[6,44,45].

3.3. Implementation Details

Our experiments were primarily conducted on the official GitHub repositories of PatchCore and BTF. Except for experimental variables and specifically mentioned parameters, all other parameters remained the same as the official defaults. Even during the performance comparison process, we abandoned many performance optimization techniques, with significant potential performance improvements.

When comparing the performance of AD&S on the MVTec-3D AD dataset using the BTM method with other approaches, we employed the parameter $k = 3$ as recommended in the PatchCore paper for the AS task in kNN)squared distance mean metrics.

3.4. Performance Comparison

3.4.1. Anomaly Detection on MVTec-3D AD

To compare the anomaly detection (AD) performance, we evaluated BTM against several 3D, RGB, and RGB + 3D multimodal methods on the MVTec-3D dataset. As shown in Table 1, under the RGB + 3D multimodal setting, BTM exhibited an average AD performance improvement of 5.7% compared to the previous BTF method; this advantage was also observed in each individual category. In the RGB and 3D modalities, BTM achieved average performance improvements of 3.1% and 3.9%, respectively, over BTF; again, this improvement was consistent across each category.

Table 1. I-AUROC score for anomaly detection of all categories of MVTec-3D AD.Our method clearly outperforms other methods in 3D and 3D + RGB setting; For pure 3D setting, our method reaches 0.874 mean I-AUROC score, and for 3D + RGB setting, we get 0.945 mean I-AUROC score. The baseline results are derived from the respective cited papers.

Method	Bagel	Cable Gland	Carrot	Cookie	Dowel	Foam	Peach	Potato	Rope	Tire	Mean
3D	Depth GAN [41]	0.538	0.372	0.580	0.603	0.430	0.534	0.642	0.601	0.443	0.532
	Depth AE [41]	0.648	0.502	0.650	0.488	0.805	0.522	0.712	0.529	0.540	0.595
	Depth VM [41]	0.513	0.551	0.477	0.581	0.617	0.716	0.450	0.421	0.598	0.555
	Voxel GAN [41]	0.680	0.324	0.565	0.399	0.497	0.482	0.566	0.579	0.601	0.482
	Voxel AE [41]	0.510	0.540	0.384	0.693	0.446	0.632	0.550	0.494	0.721	0.413
	Voxel VM [41]	0.553	0.772	0.484	0.701	0.751	0.578	0.480	0.466	0.689	0.611
	3D-ST	0.862	0.484	0.832	0.894	0.848	0.663	0.763	0.687	0.958	0.486
	M3DM [45]	0.941	0.651	0.965	0.969	0.905	0.760	0.880	0.974	0.926	0.765
	PPFH(BTF) [44]	0.820	0.533	0.877	0.769	0.718	0.574	0.774	0.895	0.990	0.582
RGB	PPFH(BTM)	0.939	0.553	0.916	0.844	0.823	0.588	0.718	0.928	0.976	0.633
	PatchCore [45]	0.876	0.880	0.791	0.682	0.912	0.701	0.695	0.618	0.841	0.702
	M3DM [45]	0.944	0.918	0.896	0.749	0.959	0.767	0.919	0.648	0.938	0.767
	RGB iNet(BTF) [44]	0.854	0.840	0.824	0.687	0.974	0.716	0.713	0.593	0.920	0.724
RGB+3D	RGB iNet(BTM)	0.909	0.895	0.838	0.745	0.975	0.714	0.79	0.605	0.93	0.759
	Depth GAN [41]	0.530	0.376	0.607	0.603	0.497	0.484	0.595	0.489	0.536	0.521
	Depth AE [41]	0.468	0.731	0.497	0.673	0.534	0.417	0.485	0.549	0.564	0.546
	Depth VM [41]	0.510	0.542	0.469	0.576	0.609	0.699	0.450	0.419	0.668	0.520
	Voxel GAN [41]	0.383	0.623	0.474	0.639	0.564	0.409	0.617	0.427	0.663	0.577
	Voxel AE [41]	0.693	0.425	0.515	0.790	0.494	0.558	0.537	0.484	0.639	0.583
	Voxel VM [41]	0.750	0.747	0.613	0.738	0.823	0.693	0.679	0.652	0.609	0.690
	M3DM*	0.998	0.894	0.96	0.963	0.954	0.901	0.958	0.868	0.962	0.797
	BTF [44]	0.938	0.765	0.972	0.888	0.960	0.664	0.904	0.929	0.982	0.726
	BTM	0.980	0.860	0.980	0.963	0.978	0.726	0.958	0.953	0.980	0.926

* Denotes results obtained by employing pre-trained parameters provided by the original studies. Unannotated results are directly excerpted from the corresponding literature.

We also replicated M3DM using the code and corresponding model parameters from the official GitHub repository. In comparing our results with the replication, our method demonstrated strong competitiveness overall. Specifically, in the RGB + 3D multimodal setting, BTM outperformed M3DM by 0.4%, achieving a performance of 93%. It is worth noting that unlike M3DM, we did not use manually designed foreground templates, leaving significant room for further AD performance enhancement. We prefer to validate the model by preserving the foreground and background to ensure its robustness.

3.4.2. Anomaly Segmentation on MVTec-3D AD

To compare the anomaly scoring (AS) performance, we evaluated BTM against several 3D, RGB, and RGB + 3D multimodal methods on the MVTec-3D dataset. As shown in Table 2, under the RGB + 3D multimodal setting, BTM achieved an average AUPRO performance of 96.9%, surpassing M3DM and BTF by 0.8% and 0.5%, respectively. This superiority was also evident when examining individual categories. In the RGB and 3D modalities, BTM outperformed BTF. It also shows strong competitiveness compared to other methods.

Table 2. AUPRO score for anomaly detection of all categories of MVTec-3D AD. Our method clearly outperforms other methods in 3D and 3D + RGB setting; For pure 3D setting, our method reaches 0.874 mean I-AUROC score, and for 3D + RGB setting, we get 0.945 mean AUPRO score. The baseline results are derived from the respective cited papers.

	Method	Bagel	Cable Gland	Carrot	Cookie	Dowel	Foam	Peach	Potato	Rope	Tire	Mean
3D	Depth GAN[41]	0.111	0.072	0.212	0.174	0.160	0.128	0.003	0.042	0.446	0.075	0.143
	Depth AE[41]	0.147	0.069	0.293	0.217	0.207	0.181	0.164	0.066	0.545	0.142	0.203
	Depth VM[41]	0.280	0.374	0.243	0.526	0.485	0.314	0.199	0.388	0.543	0.385	0.374
	Voxel GAN[41]	0.440	0.453	0.875	0.755	0.782	0.378	0.392	0.639	0.775	0.389	0.583
	Voxel AE[41]	0.260	0.341	0.581	0.351	0.502	0.234	0.351	0.658	0.015	0.185	0.348
	Voxel VM[41]	0.453	0.343	0.521	0.697	0.680	0.284	0.349	0.634	0.616	0.346	0.492
	3D-ST[42]	0.950	0.483	0.986	0.921	0.905	0.632	0.945	0.988	0.976	0.542	0.833
	M3DM [45]	0.943	0.818	0.977	0.882	0.881	0.743	0.958	0.974	0.95	0.929	0.906
	FPFH(BTF) [44]	0.972	0.849	0.981	0.939	0.963	0.693	0.975	0.981	0.980	0.949	0.928
	FPFH(BTM)	0.974	0.861	0.981	0.937	0.959	0.661	0.978	0.983	0.98	0.947	0.926
RGB	PatchCore [45]	0.901	0.949	0.928	0.877	0.892	0.563	0.904	0.932	0.908	0.906	0.876
	M3DM [45]	0.952	0.972	0.973	0.891	0.932	0.843	0.97	0.956	0.968	0.966	0.942
	RGB iNet(BTF) [44]	0.898	0.948	0.927	0.872	0.927	0.555	0.902	0.931	0.903	0.899	0.876
	RGB iNet(BTM)	0.901	0.958	0.942	0.905	0.951	0.615	0.906	0.938	0.927	0.916	0.896
RGB+3D	Depth GAN[41]	0.421	0.422	0.778	0.696	0.494	0.252	0.285	0.362	0.402	0.631	0.474
	Depth AE[41]	0.432	0.158	0.808	0.491	0.841	0.406	0.262	0.216	0.716	0.478	0.481
	Depth VM[41]	0.388	0.321	0.194	0.570	0.408	0.282	0.244	0.349	0.268	0.331	0.335
	Voxel GAN[41]	0.664	0.620	0.766	0.740	0.783	0.332	0.582	0.790	0.633	0.483	0.639
	Voxel AE[41]	0.467	0.750	0.808	0.550	0.765	0.473	0.721	0.918	0.019	0.170	0.564
	Voxel VM[41]	0.510	0.331	0.413	0.715	0.680	0.279	0.300	0.507	0.611	0.366	0.471
	M3DM*	0.966	0.971	0.978	0.949	0.941	0.92	0.977	0.967	0.971	0.973	0.961
	BTF [44]	0.976	0.967	0.979	0.974	0.971	0.884	0.976	0.981	0.959	0.971	0.964
	BTM	0.979	0.972	0.980	0.976	0.977	0.905	0.978	0.982	0.968	0.975	0.969

* Denotes results obtained by employing pre-trained parameters provided by the original studies. Unannotated results are directly excerpted from the corresponding literature.

On the MVTec-3D dataset, BTM achieved an average P-AUROC performance of 99.5%, surpassing BTF and M3DM by 0.5% and 0.2%, respectively. Detailed P-AUROC performance comparisons are provided in Table 3.

Table 3. P-AUROC score for anomaly detection of all categories of MVTec-3D AD. Our method clearly outperforms other methods in 3D and 3D + RGB setting; For pure 3D setting, our method reaches 0.874 mean P-AUROC score, and for 3D + RGB setting, we get 0.945 mean P-AUROC score. The baseline results are derived from the respective cited papers.

	Method	Bagel	Cable Gland	Carrot	Cookie	Dowel	Foam	Peach	Potato	Rope	Tire	Mean
3D	M3DM [45]	0.981	0.949	0.997	0.932	0.959	0.925	0.989	0.995	0.994	0.981	0.970
	FPFH(BTF) [44]	0.995	0.955	0.998	0.971	0.993	0.911	0.995	0.999	0.998	0.988	0.980
	FPFH(BTM)	0.995	0.96	0.998	0.97	0.991	0.894	0.996	0.999	0.998	0.987	0.979
RGB	PatchCore [45]	0.983	0.984	0.980	0.974	0.972	0.849	0.976	0.983	0.987	0.977	0.967
	M3DM [45]	0.992	0.990	0.994	0.977	0.983	0.955	0.994	0.990	0.995	0.994	0.987
	RGB iNet(BTF) [44]	0.983	0.984	0.980	0.974	0.985	0.836	0.976	0.982	0.989	0.975	0.966
	RGB iNet(BTM)	0.984	0.987	0.984	0.979	0.991	0.872	0.976	0.983	0.992	0.979	0.973
RGB+3D	M3DM*	0.994	0.994	0.997	0.985	0.985	0.98	0.996	0.994	0.997	0.995	0.992
	BTF [44]	0.996	0.991	0.997	0.995	0.995	0.972	0.996	0.998	0.995	0.994	0.993
	BTM	0.997	0.993	0.998	0.995	0.996	0.979	0.997	0.999	0.996	0.995	0.995

* Denotes results obtained by employing pre-trained parameters provided by the original studies. Unannotated results are directly excerpted from the corresponding literature.

Similarly, as we did not utilize manually designed foreground templates like M3DM or 3D-ST, we believe there is substantial room for AS performance improvement.

3.5. Performance of kNN Reweight Metrics on BTF

We conducted experiments on computing AD anomaly scores using BTF with a kNN reweighting approach (Equestrian 7) on the MVTec-3D AD dataset. As shown in Figure 8, the AD performance is lowest when k=1. Subsequently, as k increases, the influence of weight w decreases, and the AD performance gradually approaches our optimal performance.

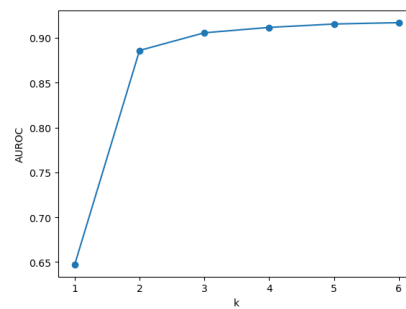
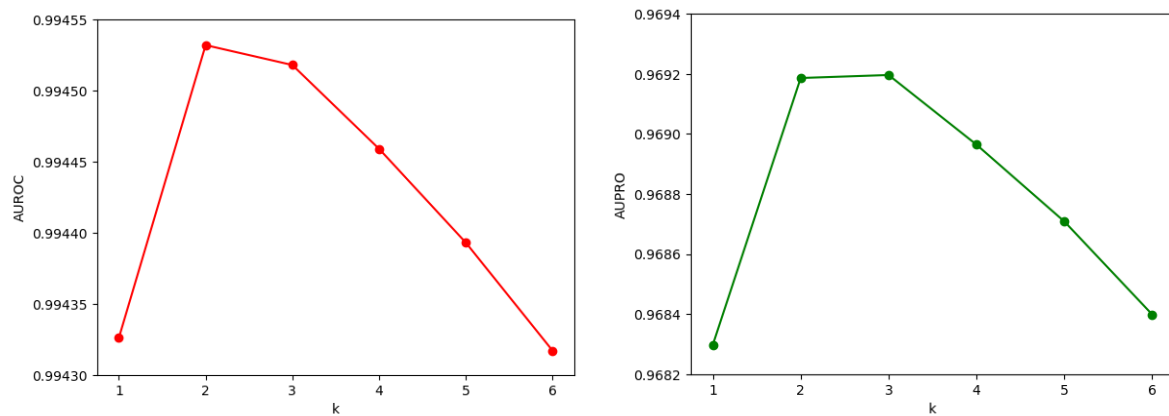


Figure 8. AD (I-AUROC) performance of kNN reweight metrics on BTF.

3.6. Performance of kNN Squared Distance Mean Metrics on BTF

We conducted experiments on computing AS anomaly scores based on kNN Squared Distance Mean Metrics using BTF on the MVTEC-3D AD dataset. As shown in Figure 9, when $k=1$, the performance of P-AUROC and AUPRO is the lowest, and then, with the increase of k , the performance of P-AUROC and AUPRO reaches the maximum at $k=2$ and $k=3$ respectively, and then continues to decrease.



(a) P-AUROC performance of kNN square distance mean metrics method on BTF.

(b) AUPRO performance of kNN square distance mean metrics method on BTF.

Figure 9. AD performance of kNN square distance mean metrics method on BTF.

4. Discussion

In Section 2.3, we analyze the kNN distance metric score distribution gradient. Through this, we find that k needs to be smaller than the number of samples in the "cluster" (defined in Section 2.1) when calculating the anomaly score using the kNN distance metric. Anomaly detection performance is best when k is close to the number of samples in the "cluster". Based on this finding, we design a simple anomaly score calculation method based on BTF, which uses different kNN metrics in AD and AS phases respectively, and name it BTM in Section 2.1. It is worth noting that more complex distance measures are worth further research. At the same time, when studying the distance metric, we should also consider the impact of the memory bank sampling method on the distance metric.

In Section 3.4, we verify the effectiveness of BTM through experiments on the real dataset MVTEC-3D AD. BTM achieves excellent performance (I-AUROC 93.0%, AUPRO 96.9%, P-AUROC 99.5%) ahead of the BTF method (I-AUROC 5.7% \uparrow , AUPRO 0.5% \uparrow , P-AUROC 0.2% \uparrow). Without using a foreground mask, BTM is still highly competitive compared to other state-of-the-art methods using manual foreground masks.

In sections 3.5 and 3.6, we further analyze "the effect of different k values on the two distance measures" and "the different effect of different k values on the AD and AS tasks" on real datasets. Further verify our conjecture in Section 2.3.

5. Conclusions

Different "clusters" have different requirements for the k value in kNN distance metrics. AD and AS tasks have different requirements for the value of k in the kNN distance metric. We designed the BTM method based on the BTF and performed experiments on MVTEC-3D AD to verify this. We also call for further research on "More complex Distance Measures" and "The Impact of memory bank's Sampling Method on Distance Measures".

Author Contributions: Conceptualization, Yujing Lin; Formal analysis, Yujing Lin; Funding acquisition, Xiaoqiang Li; Investigation, Yujing Lin; Methodology, Yujing Lin; Resources, Yujing Lin and Xiaoqiang Li; Software, Yujing Lin; Supervision, Xiaoqiang Li; Validation, Yujing Lin; Visualization, Yujing Lin; Writing – original draft, Yujing Lin; Writing – review & editing, Xiaoqiang Li.

Funding: This research received no external funding.

Institutional Review Board Statement: Not applicable.

Informed Consent Statement: Not applicable.

Data Availability Statement: In this manuscript, the employed datasets have been taken with license agreements from the corresponding institutions with proper channels.

Acknowledgments: I would like to express my heartfelt thanks to my tutor Xiaoqiang Li, Ms. Jiayuem Han and Mr. Jide Li for their guidance on this paper.

Conflicts of Interest: The authors declare no conflict of interest.

Abbreviations

The following abbreviations are used in this manuscript:

MDPI	Multidisciplinary Digital Publishing Institute
SVDD	Support Vector Data Description
GAN	Generative Adversarial Network

Appendix A. Formula Mentioned in the Original Article of PatchCore

Appendix A.1. Expressed in the Original Article

$$\begin{aligned} (m^{test,*}, m^*) &= \arg \max_{m^{test} \in \mathcal{P}(x^{test})} \arg \min_{m \in \mathcal{M}} \|m^{test} - m\|_2 \\ s^* &= \|m^{test,*} - m^*\|_2 \end{aligned} \quad (A1)$$

Appendix A.2. Expressed in Our Context

$$\begin{aligned} (f_{i^*,j^*}, m^*) &= \arg \max_{f \in F} \arg \min_{m \in \mathcal{M}} \|m - f\|_2 \\ s^* &= \|m^* - f_{i^*,j^*}\|_2 \end{aligned} \quad (A2)$$

References

1. Chandola, V.; Banerjee, A.; Kumar, V. Anomaly detection: A survey. *ACM computing surveys (CSUR)* **2009**, *41*, 1–58.
2. Ruff, L.; Kauffmann, J.R.; Vandermeulen, R.A.; Montavon, G.; Samek, W.; Kloft, M.; Dietterich, T.G.; Müller, K.R. A unifying review of deep and shallow anomaly detection. *Proceedings of the IEEE* **2021**, *109*, 756–795.
3. Rippel, O.; Merhof, D. Anomaly Detection for Automated Visual Inspection: A Review. *Bildverarbeitung in der Automation: Ausgewählte Beiträge des Jahreskolloquiums BVAu 2022* **2023**, pp. 1–13.
4. Liu, J.; Xie, G.; Wang, J.; Li, S.; Wang, C.; Zheng, F.; Jin, Y. Deep industrial image anomaly detection: A survey. *Machine Intelligence Research* **2024**, *21*, 104–135.

5. Bergmann, P.; Fauser, M.; Sattlegger, D.; Steger, C. MVTec AD—A comprehensive real-world dataset for unsupervised anomaly detection. *Proceedings of the IEEE/CVF conference on computer vision and pattern recognition*, 2019, pp. 9592–9600.
6. Bergmann, P.; Batzner, K.; Fauser, M.; Sattlegger, D.; Steger, C. The MVTec anomaly detection dataset: a comprehensive real-world dataset for unsupervised anomaly detection. *International Journal of Computer Vision* **2021**, *129*, 1038–1059.
7. Mishra, P.; Verk, R.; Fornasier, D.; Piciarelli, C.; Foresti, G.L. VT-ADL: A vision transformer network for image anomaly detection and localization. *2021 IEEE 30th International Symposium on Industrial Electronics (ISIE)*. IEEE, 2021, pp. 01–06.
8. Huang, Y.; Qiu, C.; Yuan, K. Surface defect saliency of magnetic tile. *The Visual Computer* **2020**, *36*, 85–96.
9. Bergmann, P.; Batzner, K.; Fauser, M.; Sattlegger, D.; Steger, C. Beyond dents and scratches: Logical constraints in unsupervised anomaly detection and localization. *International Journal of Computer Vision* **2022**, *130*, 947–969.
10. Li, C.L.; Sohn, K.; Yoon, J.; Pfister, T. Cutpaste: Self-supervised learning for anomaly detection and localization. *Proceedings of the IEEE/CVF conference on computer vision and pattern recognition*, 2021, pp. 9664–9674.
11. Zavrtanik, V.; Kristan, M.; Skočaj, D. Draem-a discriminatively trained reconstruction embedding for surface anomaly detection. *Proceedings of the IEEE/CVF International Conference on Computer Vision*, 2021, pp. 8330–8339.
12. Liu, Z.; Zhou, Y.; Xu, Y.; Wang, Z. Simplenet: A simple network for image anomaly detection and localization. *Proceedings of the IEEE/CVF Conference on Computer Vision and Pattern Recognition*, 2023, pp. 20402–20411.
13. Schlüter, H.M.; Tan, J.; Hou, B.; Kainz, B. Natural synthetic anomalies for self-supervised anomaly detection and localization. *European Conference on Computer Vision*. Springer, 2022, pp. 474–489.
14. Dai, S.; Wu, Y.; Li, X.; Xue, X. Generating and reweighting dense contrastive patterns for unsupervised anomaly detection. *Proceedings of the AAAI Conference on Artificial Intelligence*, 2024, Vol. 38, pp. 1454–1462.
15. Ye, Z.; Chen, Y.; Zheng, H. Understanding the effect of bias in deep anomaly detection. *arXiv preprint arXiv:2105.07346* **2021**.
16. Rippel, O.; Mertens, P.; König, E.; Merhof, D. Gaussian anomaly detection by modeling the distribution of normal data in pretrained deep features. *IEEE Transactions on Instrumentation and Measurement* **2021**, *70*, 1–13.
17. Rippel, O.; Mertens, P.; Merhof, D. Modeling the distribution of normal data in pre-trained deep features for anomaly detection. *2020 25th International Conference on Pattern Recognition (ICPR)*. IEEE, 2021, pp. 6726–6733.
18. Cordier, A.; Missaoui, B.; Gutierrez, P. Data refinement for fully unsupervised visual inspection using pre-trained networks. *arXiv preprint arXiv:2202.12759* **2022**.
19. Yoon, J.; Sohn, K.; Li, C.L.; Arik, S.O.; Lee, C.Y.; Pfister, T. Self-supervise, refine, repeat: Improving unsupervised anomaly detection. *arXiv preprint arXiv:2106.06115* **2021**.
20. Davletshina, D.; Melnychuk, V.; Tran, V.; Singla, H.; Berrendorf, M.; Faerman, E.; Fromm, M.; Schubert, M. Unsupervised anomaly detection for X-ray images. *arXiv preprint arXiv:2001.10883* **2020**.
21. Nguyen, D.T.; Lou, Z.; Klar, M.; Brox, T. Anomaly detection with multiple-hypotheses predictions. *International Conference on Machine Learning*. PMLR, 2019, pp. 4800–4809.
22. Sakurada, M.; Yairi, T. Anomaly detection using autoencoders with nonlinear dimensionality reduction. *Proceedings of the MLSDA 2014 2nd workshop on machine learning for sensory data analysis*, 2014, pp. 4–11.
23. Pidhorskyi, S.; Almohsen, R.; Doretto, G. Generative probabilistic novelty detection with adversarial autoencoders. *Advances in neural information processing systems* **2018**, *31*.
24. Sabokrou, M.; Khalooei, M.; Fathy, M.; Adeli, E. Adversarially learned one-class classifier for novelty detection. *Proceedings of the IEEE conference on computer vision and pattern recognition*, 2018, pp. 3379–3388.

25. Akcay, S.; Atapour-Abarghouei, A.; Breckon, T.P. Ganomaly: Semi-supervised anomaly detection via adversarial training. *Computer Vision–ACCV 2018: 14th Asian Conference on Computer Vision, Perth, Australia, December 2–6, 2018, Revised Selected Papers, Part III* 14. Springer, 2019, pp. 622–637.
26. Rudolph, M.; Wandt, B.; Rosenhahn, B. Same same but different: Semi-supervised defect detection with normalizing flows. *Proceedings of the IEEE/CVF winter conference on applications of computer vision*, 2021, pp. 1907–1916.
27. Gudovskiy, D.; Ishizaka, S.; Kozuka, K. Cflow-ad: Real-time unsupervised anomaly detection with localization via conditional normalizing flows. *Proceedings of the IEEE/CVF winter conference on applications of computer vision*, 2022, pp. 98–107.
28. Rudolph, M.; Wehrbein, T.; Rosenhahn, B.; Wandt, B. Fully convolutional cross-scale-flows for image-based defect detection. *Proceedings of the IEEE/CVF Winter Conference on Applications of Computer Vision*, 2022, pp. 1088–1097.
29. Zhou, Y.; Xu, X.; Song, J.; Shen, F.; Shen, H.T. MSFlow: Multiscale Flow-Based Framework for Unsupervised Anomaly Detection. *IEEE Transactions on Neural Networks and Learning Systems* **2024**.
30. Yu, J.; Zheng, Y.; Wang, X.; Li, W.; Wu, Y.; Zhao, R.; Wu, L. Fastflow: Unsupervised anomaly detection and localization via 2d normalizing flows. *arXiv preprint arXiv:2111.07677* **2021**.
31. Ruff, L.; Vandermeulen, R.A.; Görnitz, N.; Binder, A.; Müller, E.; Müller, K.R.; Kloft, M. Deep semi-supervised anomaly detection. *arXiv preprint arXiv:1906.02694* **2019**.
32. Yi, J.; Yoon, S. Patch svdd: Patch-level svdd for anomaly detection and segmentation. *Proceedings of the Asian conference on computer vision*, 2020.
33. Reiss, T.; Cohen, N.; Bergman, L.; Hoshen, Y. Panda: Adapting pretrained features for anomaly detection and segmentation. *Proceedings of the IEEE/CVF Conference on Computer Vision and Pattern Recognition*, 2021, pp. 2806–2814.
34. Bergman, L.; Cohen, N.; Hoshen, Y. Deep nearest neighbor anomaly detection. *arXiv preprint arXiv:2002.10445* **2020**.
35. Cohen, N.; Hoshen, Y. Sub-image anomaly detection with deep pyramid correspondences. *arXiv preprint arXiv:2005.02357* **2020**.
36. Defard, T.; Setkov, A.; Loesch, A.; Audigier, R. Padim: a patch distribution modeling framework for anomaly detection and localization. *International Conference on Pattern Recognition*. Springer, 2021, pp. 475–489.
37. Roth, K.; Pemula, L.; Zepeda, J.; Schölkopf, B.; Brox, T.; Gehler, P. Towards total recall in industrial anomaly detection. *Proceedings of the IEEE/CVF Conference on Computer Vision and Pattern Recognition*, 2022, pp. 14318–14328.
38. D’oro, P.; Nasca, E.; Masci, J.; Matteucci, M. Group anomaly detection via graph autoencoders. *NIPS Workshop*, 2019, Vol. 2.
39. Hyun, J.; Kim, S.; Jeon, G.; Kim, S.H.; Bae, K.; Kang, B.J. ReConPatch: Contrastive patch representation learning for industrial anomaly detection. *Proceedings of the IEEE/CVF Winter Conference on Applications of Computer Vision*, 2024, pp. 2052–2061.
40. Muhr, D.; Affenzeller, M.; Küng, J. A Probabilistic Transformation of Distance-Based Outliers. *Machine Learning and Knowledge Extraction* **2023**.
41. Bergmann, P.; Jin, X.; Sattlegger, D.; Steger, C. The MVTec 3D-AD Dataset for Unsupervised 3D Anomaly Detection and Localization. *Proceedings of the 17th International Joint Conference on Computer Vision, Imaging and Computer Graphics Theory and Applications*. SCITEPRESS - Science and Technology Publications, 2022, pp. 202–213. doi:10.5220/0010865000003124.
42. Bergmann, P.; Sattlegger, D. Anomaly detection in 3d point clouds using deep geometric descriptors. *Proceedings of the IEEE/CVF Winter Conference on Applications of Computer Vision*, 2023, pp. 2613–2623.
43. Rudolph, M.; Wehrbein, T.; Rosenhahn, B.; Wandt, B. Asymmetric student-teacher networks for industrial anomaly detection. *Proceedings of the IEEE/CVF winter conference on applications of computer vision*, 2023, pp. 2592–2602.
44. Horwitz, E.; Hoshen, Y. Back to the feature: classical 3d features are (almost) all you need for 3d anomaly detection. *Proceedings of the IEEE/CVF Conference on Computer Vision and Pattern Recognition*, 2023, pp. 2967–2976.

45. Wang, Y.; Peng, J.; Zhang, J.; Yi, R.; Wang, Y.; Wang, C. Multimodal industrial anomaly detection via hybrid fusion. *Proceedings of the IEEE/CVF Conference on Computer Vision and Pattern Recognition*, 2023, pp. 8032–8041.
46. Zavrtanik, V.; Kristan, M.; Skočaj, D. Cheating Depth: Enhancing 3D Surface Anomaly Detection via Depth Simulation. *Proceedings of the IEEE/CVF Winter Conference on Applications of Computer Vision*, 2024, pp. 2164–2172.
47. Chu, Y.M.; Liu, C.; Hsieh, T.I.; Chen, H.T.; Liu, T.L. Shape-guided dual-memory learning for 3D anomaly detection. *Proceedings of the 40th International Conference on Machine Learning*, 2023, pp. 6185–6194.
48. Peterson, L.E. K-nearest neighbor. *Scholarpedia* **2009**, *4*, 1883.
49. Sener, O.; Savarese, S. Active Learning for Convolutional Neural Networks: A Core-Set Approach. *International Conference on Learning Representations*, 2018.

Disclaimer/Publisher's Note: The statements, opinions and data contained in all publications are solely those of the individual author(s) and contributor(s) and not of MDPI and/or the editor(s). MDPI and/or the editor(s) disclaim responsibility for any injury to people or property resulting from any ideas, methods, instructions or products referred to in the content.